Journal of Materials Processing Technology 160 (2005) 267–277

Journal of Materials Processing Technology

www.elsevier.com/locate/jmatprotec

Modelling of dynamic and metadynamic recrystallisation during bar rolling of a medium carbon spring steel

J.H. Bianchi[a,*], L.P. Karjalainen[b]

[a] *Centro Sviluppo Materiali, Via Castel Romano 100, 00128 Roma, Italy*
[b] *Department of Mechanical Engineering, University of Oulu, P.O. Box 4200, 90014 Oulu, Finland*

Received 16 July 2003; received in revised form 17 June 2004; accepted 17 June 2004

Abstract

A constitutive model for hot deformation of a medium-carbon spring steel has been developed and validated using isothermal compression experiments at monotonic and abruptly changed strain rate conditions, providing data for the flow stress and softening kinetics. The integrated deformation-softening constitutive model is based on the two hypotheses: (a) instantaneous response of the microstructure to varying temperature–strain rate conditions and (b) invariance of the kinetics of different strain states having equal effective plastic strain. It has been implemented in a FEM code and applied to bar and rod hot rolling schedules. The predictions for the plain medium-carbon steel considered indicate that dynamic (DRX) and metadynamic (MDRX) recrystallisation are possible to occur in both the roughing and finishing mills. A comparison for the same rolling schedule applied to a medium-carbon multialloyed steel shows that its higher resistance to DRX cannot prevent recrystallisation in the intermediate mill, but it can in the finishing mill if there is no significant strain accumulation.

Keywords: Bar rolling; Constitutive laws; Dynamic recrystallisation; Rolling models; Medium carbon steel

1. Introduction

The experimental possibilities of following microstructural evolution in industrial bar/rod mills at intermediate stages are very limited, because the difficulties in both cutting samples and quenching them in times short enough to freeze the austenitic microstructure. The alternative of reproducing industrial rolling conditions in pilot mills is restricted because of their smaller geometric dimensions, their slower rolling speeds and the absence of interstand tensions. The presence of dynamic recrystallisation (DRX) and metadynamic recrystallisation (MDRX) in the finishing bar/rod rolling conditions have been shown in torsion simulation tests and modelled using simple regression equations and spreadsheets [1,2]. Results from numerical simulation rolling models also support this view [3–6], while it is also suggested that the time to trigger DRX cannot be normally exceeded in the rolling pass [7,8].

The characteristics of SRX and MDRX have been discussed by Karjalainen and Perttula [9] and those of MDRX by Hodgson [10], among others. The onset and the kinetics of different softening mechanisms, DRX during deformation and static recrystallisation (SRX) or MDRX after the final pass or during interpass-times are temperature T and strain rate $\dot{\bar{\varepsilon}}$ dependent. Therefore, although the critical strain ε_d to start DRX, its associated volume fraction X_d and the post-deformation softening fraction X_s can all be identified almost uniquely (within the experimental error limitations) in isothermal tests at constant strain rates, their extrapolation to the local conditions developed in metal forming is not straightforward.

The early isotropic hardening-dynamic recovery viscoplastic model of Anand [11] has been applied to general metal forming problems on the assumption the invariants of strain, strain rate and flow stress computed from the general triaxial state are equivalent to the corresponding measures of the mechanical testing [11–17]. Post-deformation recrystallisation of austenite has been incorporated into interpass

* Corresponding author.
E-mail address: j.bianchi@c-s-m.it (J.H. Bianchi).

0924-0136/$ – see front matter © 2004 Elsevier B.V. All rights reserved.
doi:10.1016/j.jmatprotec.2004.06.016

Nomenclature

$\bar{\sigma}$	equivalent stress
$\bar{\varepsilon}$	effective plastic strain defined from its ε_{ij} components as, $\bar{\varepsilon} = [(\frac{2}{3})\varepsilon_{ij} : \varepsilon_{ij}]^{1/2}$
$\dot{\bar{\varepsilon}}$	effective strain rate defined as, $\dot{\bar{\varepsilon}} = \frac{\Delta\bar{\varepsilon}}{\Delta t}$
T	temperature
s_{def}	hardness
ε_{d}	critical strain to start DRX
X_{d}	volume fraction dynamically recrystallised
X_{s}	volume fraction statically recrystallised
t	time
D	austenite grain size
$\hat{\dot{\bar{\varepsilon}}}$	prior strain rate for SRX and MDRX
$\hat{\varepsilon}_{\text{d}}$	prior deformation critical strain from $\hat{\dot{\bar{\varepsilon}}}$
η	dimensionless fractional strain measured from ε_{d}
ε_{ch}	strain delimiting two constant strain rate testing in stepped experiments

Note: The barred measures are noted as invariants of the triaxial state, even though they represent only one component in the mechanical test

models using different measures of the prior deformation critical strain $\hat{\varepsilon}_{\text{d}}$ that defines the transition from SRX to MDRX [13,15]. Integrated rolling-interpass models have been applied to determine the effects of rolling parameters on dimensional tolerances and forces and used to derivate simplified models for on-line control [15,16]. Through-process models of complete rolling lines that consider multiple structures [4,6,13] undergoing different degrees of hardening and volume fractions percolated by grain sizes have been also developed.

The hot working characterising procedure requires constant $\dot{\bar{\varepsilon}}$ testing, which is not always attainable in the upper range of rolling conditions. In spite of this limitation, the extrapolation of the resulting constitutive and microstructural models to both range and varying patterns of strain rate predicted by FEM-based process models, is slowly entering as a powerful tool in microstructural development research.

This paper elaborates further on the rate-dependent microstructural processes and aims to aid understanding the conditions in which DRX develops in industrial bar/rod rolling. A full material characterisation of a medium-carbon steel, DIN55Cr3, has been carried out and a constitutive model that considers work hardening, dynamic recovery, dynamic recrystallisation and static softening has been developed. The constitutive model has been experimentally validated for varying $\dot{\bar{\varepsilon}} - T$ conditions, coded in a coupled temperature–stress analysis procedure of a commercial FEM code [18] and applied to typical passes of bar and rod rolling.

2. Experimental

A medium-carbon spring steel DIN55Cr3 was used with the chemical composition (wt.%) 0.55 C, 0.31 Si, 0.78 Mn, 0.76 Cr, 0.10 Cu, 0.07 Ni and 0.02 Mo. Pieces of a rolling stock were taken from the intermediate mill, examined metallographically and non-central areas having homogeneous and segregation-free microstructure were identified. From these, cylindrical specimens of 10 mm diameter and 12.5 mm height were cut and machined.

Axisymmetric compression tests at constant or abruptly changed true strain rates in the range 0.01–10 s^{-1} were carried out on a Gleeble 1500 thermo-mechanical simulator. The raw data were recorded during the full test and converted to flow stress–strain curves. The specimens were first heated up to 1050 °C for 2 min, then cooled at 2 °C/s to the testing temperature (between 950 and 1050 °C) and held for 15 s before the compression. The austenite grain size measured after the reheating was about 34 μm.

In addition, the SRX and MDRX kinetics following the various deformation histories (monotonic or changed strain rates) were determined by the stress relaxation method [9,19], to identify the most representative strain rates to be used in computing the softening rate in rolling schedules.

3. Material model for hot deformation of austenite under varying $T - \dot{\bar{\varepsilon}}$ conditions

Anand [11] and Brown et al. [17] extended the flow stress $\bar{\sigma}$ of classical hot working theory:

$$\bar{\sigma} = s_{\text{def}}\mathcal{F}(Z; m_{\text{s}}) \tag{1}$$

using a 'hardness' variable s_{def} varying between its yielding s_0 and steady state saturation $\hat{s}_{\text{s}}$ limits, with associated rate sensitivity m having limits m_0 and m_{s}, respectively. The formulation used the function:

$$\mathcal{F}(Z; m) = \text{arcsinh}\left[\left(\frac{Z}{A}\right)^{m}\right] \tag{2}$$

which has been traditionally used to fit peak stress data, in terms of the temperature-compensated strain rate, the Zener–Hollomon parameter Z:

$$Z = \dot{\bar{\varepsilon}} \exp\left(\frac{Q}{RT}\right) \tag{3}$$

where Q is the activation energy of deformation and R = 8.31 J mol^{-1} K^{-1}. In the early work, the factor s_{def} was only dependent on strain and therefore represented a sort of room temperature, non-dynamic loading value, which could be assimilated to a 'hardness' measure. The nomenclature is kept in this work, in spite that the current model exhibits some sensitivity to Z (n in Eq. (4)), resulting from m_0 and m_{s} being different.

3.1. Work hardening and dynamic recovery

Here, the hardness evolution law proposed by Anand [11], Brown et al. [17] and Estrin and Mecking [20] is generalised describing isotropic hardening and dynamic recovery as:

$$\left.\frac{\mathrm{d}s_{\mathrm{def}}}{\mathrm{d}\bar{\varepsilon}}\right|_{\mathrm{H+DRV}} = h\mathcal{F}(Z;n)\left[1-\left(\frac{s_{\mathrm{def}}}{\hat{s}_{\mathrm{s}}}\right)^{a}\right] \tag{4}$$

where h represents a pure hardening rate and n a small sensitivity to Z. Because the better fitting of Eq. (1) to the experimental values at the saturation state $\hat{s}_{\mathrm{s}}$ than at the yielding state s_0 [12], it is convenient to use the former as a reference. The hardness corresponding to yielding is next defined as:

$$s_0 = \hat{s}_0\frac{\mathcal{F}(Z;m_0)}{\mathcal{F}(Z;m_{\mathrm{s}})} \tag{5}$$

The stress at which the hardening rate given by Eq. (4) vanishes and s_{def} hits its maximum $\hat{s}_{\mathrm{s}}$, represents in Eq. (1) the 'steady state' or hypothetical flow stress in absence of DRX.

Table 1 shows the values of the parameters obtained by applying the constitutive model to the data from the monotonic compression experiments. Once the casting structure has been destroyed by rolling, the coefficient a defines the work hardening controlled by the dislocation density [11,17,20], with a value about 1. For the very first roughing passes, however, its value is higher.

Brown et al. [17] applied the model to a Fe–Si steel in a wide strain range and showed that s_{def} can be regarded as a state parameter under Z-changes conditions. However, for applications to hot rolling of steels in the *austenitic* regime, recrystallisation has to be considered and incorporated into the constitutive model.

The onset of both DRX and MDRX under constant $\dot{\bar{\varepsilon}}-T$ conditions depends on whether $\bar{\varepsilon}$ has exceeded the critical strain:

$$\varepsilon_{\mathrm{d}} = B_2 D^{\mathrm{d}} Z^{q} \tag{6}$$

Table 1
Material model parameters for the DIN55Cr3 medium-carbon steel studied

Parameter	Value
Q (J mol^{-1})	340200
A (s^{-1})	3.161310^{12}
m_{s}	0.231
m_0	0.293
n	−0.20
$\hat{s}_{\mathrm{s}}$ (MPa)	90
$\hat{s}_0$ (MPa)	40
h (MPa)	1100
a	1.0
c	0.57
d	0.5
k	1.5723
p	0.084
q	0.15
B_1 (MPa)	1.025
B_2	3.3610^{-4}

where D is in μm. The parameters determined from the monotonic compression experiments for the present steel are given in Table 1.

Contrary to the conventional mechanical testing, hot rolling deformation inevitably involves non-isothermal deformation with $\dot{\bar{\varepsilon}}$ localisations that generate non-unique ε_{d} along the material path. An approach to simulate the effects of such conditions during deformation is formulated in then next subsection, whereas their influences on post-deformation are examined in Section 5.2.

3.2. Dynamic recrystallisation

For strains exceeding the threshold given by Eq. (6), the recrystallised volume fraction X_{d} is assumed to follow the Avrami type equation:

$$X_{\mathrm{d}} = 1-\exp(-c\eta^{k}) \tag{7}$$

where η is a dimensionless fractional strain measured from the DRX onset:

$$\eta = \frac{\bar{\varepsilon}-\varepsilon_{\mathrm{d}}}{\varepsilon_{\mathrm{d}}} \tag{8}$$

In order to obtain a unique value of X_{d} for the general non-isothermal, varying strain rate case, we make the assumption that also the microstructure reacts instantaneously to the new conditions, as done previously for the hardness. This is achieved by recasting Eq. (7) into an incremental form to be integrated at the quasi-steady conditions of the very small time/strain increments resulting during the FEM metal forming analysis. The recrystallised fraction $X_{\mathrm{d}}(i)$ at a given i-strain is obtained by applying the recursive relationship:

$$X_{\mathrm{d}}{}^{(i)} = X_{\mathrm{d}}{}^{(i-1)} + \frac{\mathrm{d}X_{\mathrm{d}}}{\mathrm{d}\bar{\varepsilon}}\mathrm{d}\varepsilon \tag{9}$$

and enforcing the additivity of the recrystallisation rates from different $\dot{\bar{\varepsilon}}$–T conditions by using the fraction at the end of the previous incremental step $X_{\mathrm{d}}(i-1)$ in the rate:

$$\frac{\mathrm{d}X_{\mathrm{d}}}{\mathrm{d}\bar{\varepsilon}} = \mathcal{H}(\eta)(1-X_{\mathrm{d}}{}^{(i-1)})\frac{ck\eta^{k-1}}{\varepsilon_{\mathrm{d}}} \tag{10}$$

where DRX contributions are only activated for $\eta > 0$:

$$\begin{aligned}\mathcal{H}(\eta) &= 1 \quad \text{for} \quad \eta > 0\\ \mathcal{H}(\eta) &= 0 \quad \text{for} \quad \eta < 0\end{aligned} \tag{11}$$

A quantification of purely DRX effects on the flow stress is obtained by the procedure that follows. First, the experimental flow stress for each constant $\dot{\bar{\varepsilon}}-T$ test is compared against the steady state stress associated to the $\hat{s}_{\mathrm{s}}$ parameter determined by the hardening-dynamic recovery model of Section 3.1. The resulting stress difference is correlated to the evolving strain for each test, with individual coefficients that are finally correlated to the $\dot{\bar{\varepsilon}}-T$ conditions over the whole set of tests. Finally, the resulting expression for the flow stress

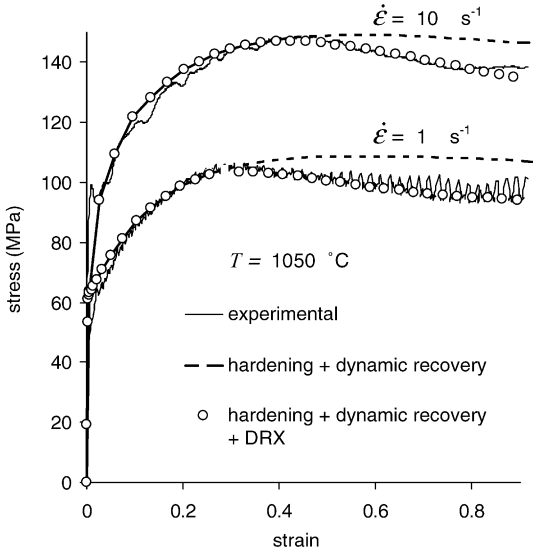

Fig. 1. Comparison between experimental and predicted flow stresses for two monotonic compression tests at 1050 °C, as accounting for different processes.

difference is recast in the general framework of Eqs. (1) and (4) with a modified hardening rate that incorporates DRX:

$$\left.\frac{\mathrm{d}s_{\mathrm{def}}}{\mathrm{d}\bar{\varepsilon}}\right|_{H+\mathrm{DRV}+\mathrm{DRX}} = \left.\frac{\mathrm{d}s_{\mathrm{def}}}{\mathrm{d}\bar{\varepsilon}}\right|_{H+\mathrm{DRV}} - \mathcal{B}(Z)\frac{\mathrm{d}X_{\mathrm{d}}}{\mathrm{d}\bar{\varepsilon}} \tag{12}$$

with

$$\mathcal{B}(Z) = B_1 \frac{Z^p}{\mathcal{F}(Z; m_{\mathrm{s}})} \tag{13}$$

The DRX model parameters obtained for the present steel are also given in Table 1.

Fig. 1 shows a comparison between the experimental and FEM-computed stress–strain curves for two typical characterising tests. The dotted line corresponds to the hypothetical maximum stress associated to the hardness saturation $\hat{s}_{\mathrm{s}}$, asymptotically reached by integration of Eq. (4). The small drop in this stress is attributed to the temperature rise due to adiabatic heating at high strain rates. In the full model resulting from the integration of Eq. (12), it is seen that the flow stress levels off further by the activation of DRX described by Eq. (10). The predictions fit well the experimental curves up to about 0.85 strain.

4. Experimental validation of the hypothesis of hardness as a state variable

The validity of the instantaneous response hypothesis was next explored by additional Gleeble compression experiments in which the constant strain rate was abruptly changed at a certain strain $\varepsilon_{\mathrm{ch}}$. Fig. 2 shows the results obtained at 1050 °C, together with the stress–strain curves obtained at monotonic constant strain rates. Within the experimental

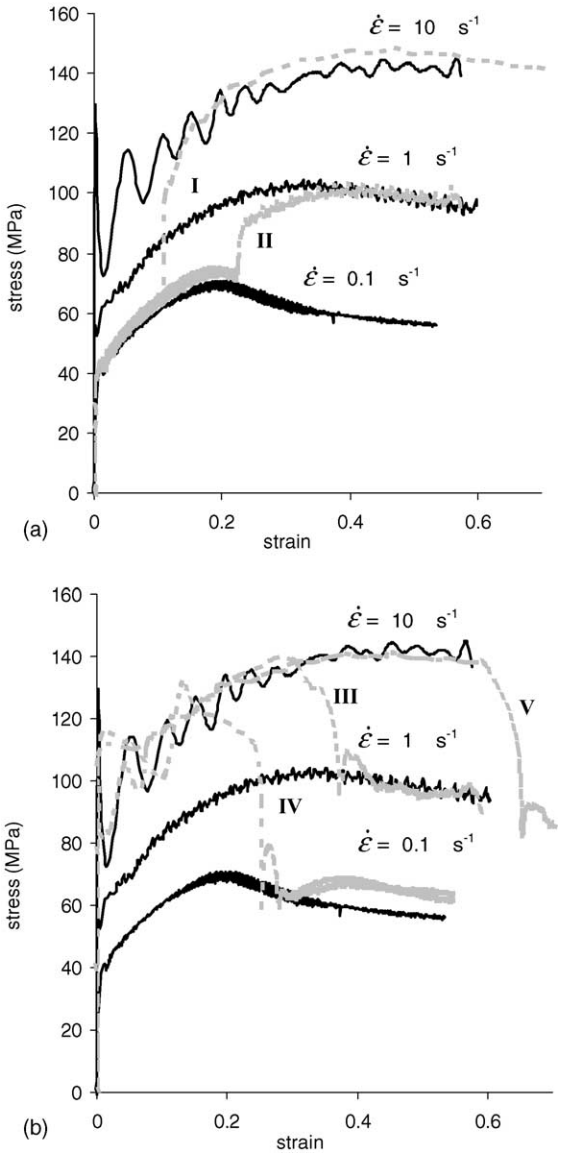

Fig. 2. Flow stress curves at 1050 °C at single strain rate and two constant strain rates with an abrupt change at strain $\varepsilon_{\mathrm{ch}}$: (a) increasing (b) decreasing stepped strain rates.

scatter, the flow stress of the second $\dot{\bar{\varepsilon}}$ regime tends to approach asymptotically the single-$\dot{\bar{\varepsilon}}$ curve. There is always a short transient that is the composite effect of the strain at which the applied $\dot{\bar{\varepsilon}}$ stabilises at its new value, dependent on the response of the Gleeble simulator, and a purely material response lagging behind the mechanical state, as discussed elsewhere [24,25].

Under increasing $\dot{\bar{\varepsilon}}$ conditions (Fig. 2a), the response is almost instantaneous if the strain rate change occurs in the work hardening-dynamic recovery region of both $\dot{\bar{\varepsilon}}$ regimes (I, $\varepsilon_{\mathrm{ch}} = 0.1$). The transient is longer if $\varepsilon_{\mathrm{ch}}$ is in the DRX region of the first stage but corresponds to the hardening-dynamic recovery area of the second stage (II, $\varepsilon_{\mathrm{ch}} = 0.22$). It is now well known from FEM analysis that rolling deformation involves a

high $\dot{\bar{\varepsilon}}$ raise on entering the roll gap [12–15], conditions which resemble the curve (I) with a continuous transition across the hardening-dynamic recovery region at different rates.

FEM rolling simulations also predict a fast decay of $\dot{\bar{\varepsilon}}$ within the deformation zone after peaking, conditions which are explored by the experiments shown in Fig. 2b. Due to the reduction of the instantaneous strain ε_d with decreasing strain rate $\dot{\bar{\varepsilon}}$ (Eq. (6)), a change of this started in the hardening-dynamic recovery region easily falls in the DRX region of the second constant strain rate (III and IV). The asymptotic approach towards the corresponding second $\dot{\bar{\varepsilon}}$ is evident if ε_{ch} occurs under predominantly DRX conditions (III, ε_{ch} = 0.30–0.35). If the second $\dot{\bar{\varepsilon}}$ is very low (IV, ε_{ch} = 0.15–0.25), softening is extremely fast followed by a new work hardening cycle [24]. If the ε_{ch} change takes place in the DRX region (V, ε_{ch} = 0.6–0.65), the flow stress also approaches asymptotically the lower constant $\dot{\bar{\varepsilon}}$ curve after a short transient.

5. Interpass recrystallisation

5.1. Results from constant $T - \dot{\bar{\varepsilon}}$ conditions

The stress relaxation testing constitutes a powerful technique to obtain the recrystallised volume fraction X_s during holding times following the deformation by a limited number of experiments [9,19]. For the medium-carbon steel under study, the stress relaxation data obtained by the experiments were fitted by the Avrami-type equation:

$$X_s = 1 - \exp\left[-\beta\left(\frac{t}{t_{0.5}}\right)^b\right] \tag{14}$$

in term of the post deformation elapsed time t and the reference time $t_{0.5}$, time for 50% recrystallised fraction, with coefficients $\beta = 0.693$ and $b \sim 1.5$.

Using a regression analysis, two expressions for $t_{0.5}$ were obtained in terms of the prior strain:

SRX regime ($\bar{\varepsilon} \le \varepsilon_d$):

$$t_{0.5} = 2.75\,10^{-11}\, D^{1.06}\, \varepsilon^{-2.45}\, \dot{\bar{\varepsilon}}^{-0.125} \exp\left(\frac{184000}{RT}\right) \tag{15}$$

MDRX region ($\bar{\varepsilon} > \varepsilon_d$)

$$t_{0.5} = 3.59\,10^{-2}\, \dot{\bar{\varepsilon}}^{-0.785} \exp\left(\frac{24800}{RT}\right) \tag{16}$$

5.2. Influence of varying $T - \dot{\bar{\varepsilon}}$ conditions on the subsequent recrystallisation kinetics

The empirical expression given by Eq. (15) shows that the reference time $t_{0.5}$ defining the rate of SRX is dependent on the grain size, strain and temperature, with a minimum strain rate influence. The MDRX rate associated to Eq. (16) in turn, is more dependent on strain rate and slightly on temperature. Strictly speaking, $t_{0.5}$ is related to the past strain rates and an evolving temperature T, this not necessarily being equal to that at which the deformation was applied. In fact, preferably Z instead of the strain rate should be used in Eqs. (15) and (16). Anyhow, because the strain rate dependence of both $t_{0.5}$ and ε_d, the general deformation case requires to define critical strain $\hat{\varepsilon}_d$ and strain rate $\hat{\dot{\bar{\varepsilon}}}$ measures that are representative of the varying conditions of the past deformation.

5.2.1. Defining a prior strain rate $\hat{\dot{\bar{\varepsilon}}}$ for the reference time $t_{0.5}$

In previous works [13,15] two strain rate measures obtained from upstream values in the path were explored:

$$\hat{\dot{\bar{\varepsilon}}} = \dot{\bar{\varepsilon}}_{max} = \text{maximum strain rate} \tag{17}$$

and the strain average computed as

$$\hat{\dot{\bar{\varepsilon}}} = \dot{\bar{\varepsilon}}_{strain-average} = \frac{\sum \dot{\bar{\varepsilon}}\,\Delta\varepsilon}{\bar{\varepsilon}_{pass}} \tag{18}$$

where $\bar{\varepsilon}_{pass}$ is the effective total strain in the pass being considered. Here, we introduce the time average:

$$\hat{\dot{\bar{\varepsilon}}} = \dot{\bar{\varepsilon}}_{time-average} = \frac{\sum \dot{\bar{\varepsilon}}\,\Delta t}{t_{pass}} \tag{19}$$

where t_{pass} is the total time taken by the pass-deformation.

5.2.2. Defining the $\hat{\varepsilon}_d$ strain delimiting SRX–MDRX regions

MDRX starts from the nuclei formed during deformation. In the past Bianchi [13] and Bianchi and co-workers [13,15], have introduced the $\hat{\dot{\bar{\varepsilon}}}$ definitions above to compute the DRX strain (Eq. (6)) as:

$$\hat{\varepsilon}_d = \varepsilon_d(\dot{\bar{\varepsilon}}_{max}) \tag{20}$$

and

$$\hat{\varepsilon}_d = \varepsilon_d(\dot{\bar{\varepsilon}}_{strain-average}) \tag{21}$$

In the current work it is introduced:

$$\hat{\varepsilon}_d = \varepsilon_d(\dot{\bar{\varepsilon}}_{time-average}) \tag{22}$$

The measure in Eq. (21) gives more weight to the rates at the higher strain changes, while the lower value resulting from Eq. (22) outweighs the rate applied over longer periods of time.

A fourth possibility is given by the *first* strain value exceeding the instantaneous ε_d:

$$\hat{\varepsilon}_d = \varepsilon_d(\eta_{(1)} = 0) \tag{23}$$

where η is the fractional overstrain given by Eq. (8)) and the condition $\eta = 0$ can occur more than once when deforming across varying strain rate localizations as happens in rolling.

5.3. Multipass deformation with holding periods

In order to maintain the form of the base Eq. (1), the hardness parameter for any subsequent deformation is now written as:

$$s = s_{\text{def}}(1 - X_s) + \hat{s}_0 X_s \quad (24)$$

where the statically recrystallised volume fraction X_s is obtained by integrating the time-derivative of Eq. (14) under the generally non-isothermal conditions resulting in a transient thermal analysis of the interpass period [15]. For the sake of simplicity and considering the very fast interpass recrystallisation of the studied steel, extension to multiple microstructures [4,13] has not been considered.

6. Experimental identification of a representative prior strain rate for static softening

In order to assess the most representative strain rate $\hat{\dot{\varepsilon}}$ defining the X_s kinetics from prior deformations occurred at varying strain rates, a series of stress relaxation experiments were performed at the temperatures of 950 and 1050 °C. In accordance with typical rolling pass conditions, all the tests were carried up to total strains of about 0.5–0.6 and at decreasing $\dot{\varepsilon}$. Fig. 3 compares the evolution in time of the recrystallised volume fraction X_s resulting from abruptly changed $\dot{\varepsilon}$ conditions, against the Avrami fittings (Eq. (14)) corresponding to constant $\dot{\varepsilon}$. It is clear from the results that the recrystallisation kinetics shifts towards the side of the second, i.e. lower, strain rate.

From the experiments in which the strain rate was changed from 10 to 1 s^{-1}, the prior strain rate measures computed by Eqs. (18) and (19) are $\hat{\dot{\varepsilon}}_{\text{strain–average}} = 9\,s^{-1}$ and $\hat{\dot{\varepsilon}}_{\text{time–average}} = 1.5\,s^{-1}$. The X_s values obtained using these rates in the $t_{0.5}$ computations clearly show that the time-averaged measure, i.e. Eq. (22) gives a better approximation to the stepped-strain rate experiments that the strain-averaged measure (Eq. (21)). The time-average procedure, i.e. the mean strain rate, was also found reasonable by Karjalainen et al. [24] for a Ti-bearing steel, especially in the case of SRX and decreasing strain rate. They observed that the 'effective strain rate' was close to the final (second) strain rate.

7. Application to FEM simulation of bar/rod rolling

7.1. Case study: rolling schedule for a ϕ = 24 mm final bar

The constitutive model is next applied to the FEM simulation of the R8 round–oval pass of an intermediate mill, with an entry stock diameter of 52 mm, a bar 'area reduction' AR = 0.25, an entry T = 1040 °C and a rolling speed V

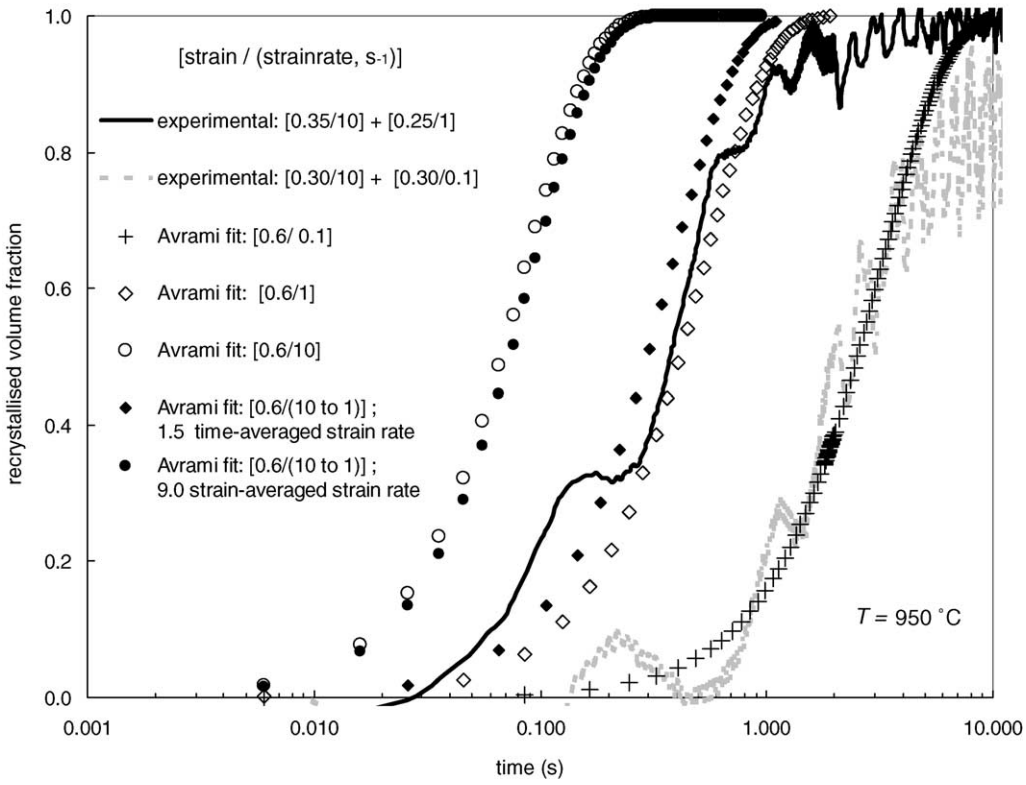

Fig. 3. Recrystallised volume fractions obtained from stepped strain rate experiments and tests at constant strain rates, as expressed by the Avrami-type curves fitted with the stress relaxation data.

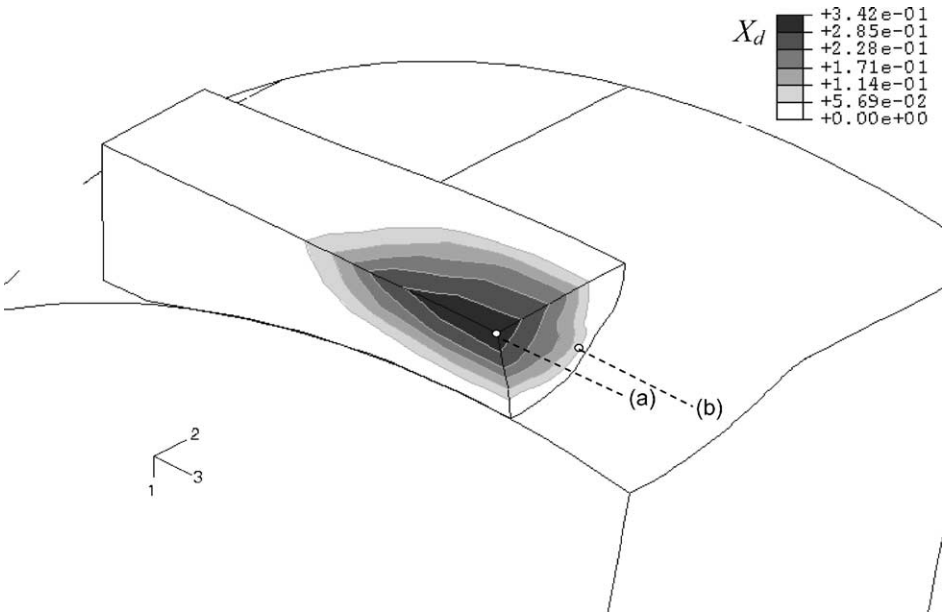

Fig. 4. Evolution of the dynamic recrystallised volume fraction X_d predicted by the present FEM model for stand R8 during a ϕ = 24 mm bar rolling schedule, with stand parameters: T = 1040 °C, V = 1.7 m s^{-1}.

of 1.7 m s^{-1}, using the process models with the parameters reported in [15].

The predicted DRX volume fraction X_d is maximum around the centreline and decreases towards the contacting surface (Fig. 4). The last result is due to the two main conditions faced by the material flowing along the border streamlines: (a) a DRX strain ε_d (Eq. (6)) higher than at the core streamline, as consequence of the T—drop produced by the chilling effects of the rolls and [15]; (b) an effective strain $\bar{\varepsilon}$ lower than at the core, which results from reversal of the shear strain components [14].

For the particular steel and rolling pass conditions examined, the FEM results in Fig. 5 for the two typical streamlines in Fig. 4 show that $\bar{\varepsilon}$ exceeds the instantaneous ε_d (Eq. 6) computed from the *local* strain rate from midway the deformation zone. This happens at the peak of the ε_d (hence strain rate) profile in the core streamline, but after a substantial decay in the border streamline (curves 1 and 2, Fig. 5). Such conditions define DRX in the pass and MDRX in the subsequent interpass. The same microstructural prediction results from the averaged and η = 0 DRX–strain measures levels (lines 4, 5, 6), which are all exceeded by the pass strain $\bar{\varepsilon}$ (curve 1). The DRX–strain measure based on the maximum strain rate predicts DRX/MDRX at the core but SRX at the border subcutaneous streamline (curves 1 and line 3).

Of particular interest is the comparison against the predictions from two Homogeneous Deformation Models (HDM). The frequently used simplistic HDM model based only on the area reduction (AR), suggests an opposite recrystallisation scenario, with the overall strain not exceeding its DRX threshold (lines 7 and 8). The improved HDM model based on equivalent rectangular sections and consistent elongation enforcing constant volume (EQR + CVEL) [22,23], predicts MDRX (lines 9 and 10) with a critical strain similar to the FEM results, but a lower mean strain.

The multiaxial deformation faced by the material during rolling is predominantly determined by normal strain components, but along the streamlines emerging near the border in contact with the tooling, non-negligible shear strain components develop. At least one of these last undergoes a reversal within the deformation zone [14,15]. The material flowing along the central streamline faces a single $\dot{\bar{\varepsilon}}$ peak while, depending on the length of the contact arc, two or more $\dot{\bar{\varepsilon}}$ peaks develop along the border lines [13,21]. The definition given by Eq. (23) retains memory of the conditions at which DRX nucleated first and therefore appears as a natural choice for identifying the SRX–DRX transition (Eqs. (15) and (16)) under the varying rate loading resulting in rolling.

Fig. 6a shows the evolution of softening with interstand travelling time, at the centre of the rolled bar section (point (A)) for different prior-$\dot{\bar{\varepsilon}}$ definitions. In spite of the differences of these rates, they all predict complete recrystallisation within interstand distance. The outer layers of the stock that contacted the cooler rolls partially recover temperature by internal conduction from the hotter inner core during the interpass time [4,15,16], but they nevertheless remain at a lower temperature that delays recrystallisation (Fig. 6b). Due to the massive area fully recrystallised, the effect of interstand softening on the rolled forces of the considered stand, for this particular steel is minimal [15,16].

7.2. Rolling schedule for a ϕ = 5.5 mm final rod: analysis of recrystallisation at the stock core streamline

In Fig. 7, the effects of the main process parameters on DRX are illustrated for three representative stands during a ϕ

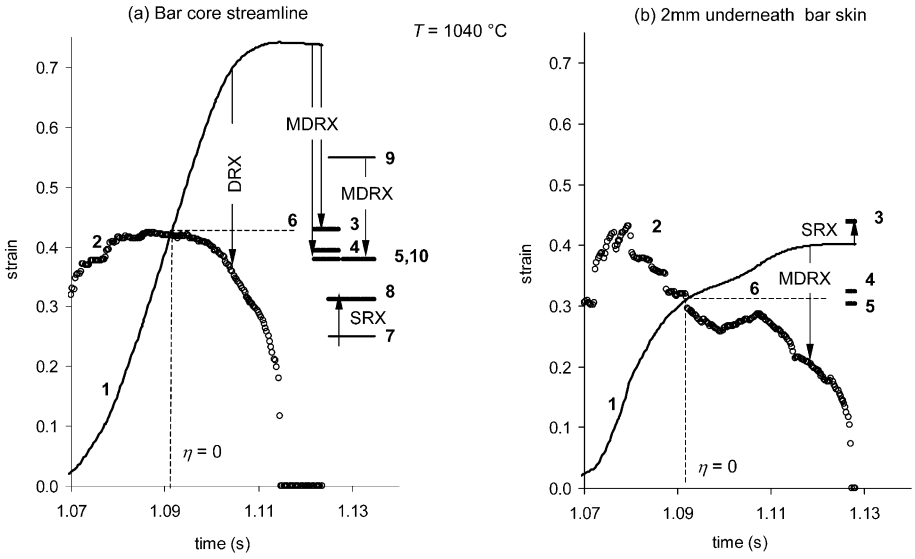

Strain Rate s^{-1}	(a)	(b)
$\dot{\bar{\varepsilon}}_{max}$	25.3	28.7
$\dot{\bar{\varepsilon}}_{strain\text{-}average}$	19.0	11.6
$\dot{\bar{\varepsilon}}_{time\text{-}average}$	15.5	8.3
$\dot{\varepsilon}_{HDM\ (AR)}$	5.2	5.2
$\dot{\varepsilon}_{HDM\ (EQR+CVEL)}$	11.5	11.5

FEM				HDM	
1	$\bar{\varepsilon}$	3	$\varepsilon_d\ (\dot{\bar{\varepsilon}}_{max})$	7	$\bar{\varepsilon}_{HDM\ (AR)}$
2	$\varepsilon_d\ (\dot{\bar{\varepsilon}}_{local})$	4	$\varepsilon_d\ (\dot{\bar{\varepsilon}}_{strain\text{-}average})$	8	$\varepsilon_d\ (\dot{\varepsilon}_{HDM(AR)})$
		5	$\varepsilon_d\ (\dot{\bar{\varepsilon}}_{time\text{-}average})$	9	$\bar{\varepsilon}_{HDM\ (EQR+CVEL)}$
		6	$\varepsilon_d\ (\eta = 0)$	10	$\varepsilon_d\ (\dot{\varepsilon}_{HDM(EQR+CVEL)})$

Fig. 5. Evolution of different strain and DRX strain measures at the two typical streamlines in Fig. 4. FEM simulation of R8 rolling stand, $T = 1040\,^{\circ}C$, $V = 1.7\,m\,s^{-1}$; HDM are homogeneous deformation models based on AR = area reduction and EQR + CVEL = equivalent rectangular area with constant volume elongation. Values of strain rates corresponding to the DRX strains levels marked as 3–10 are also shown.

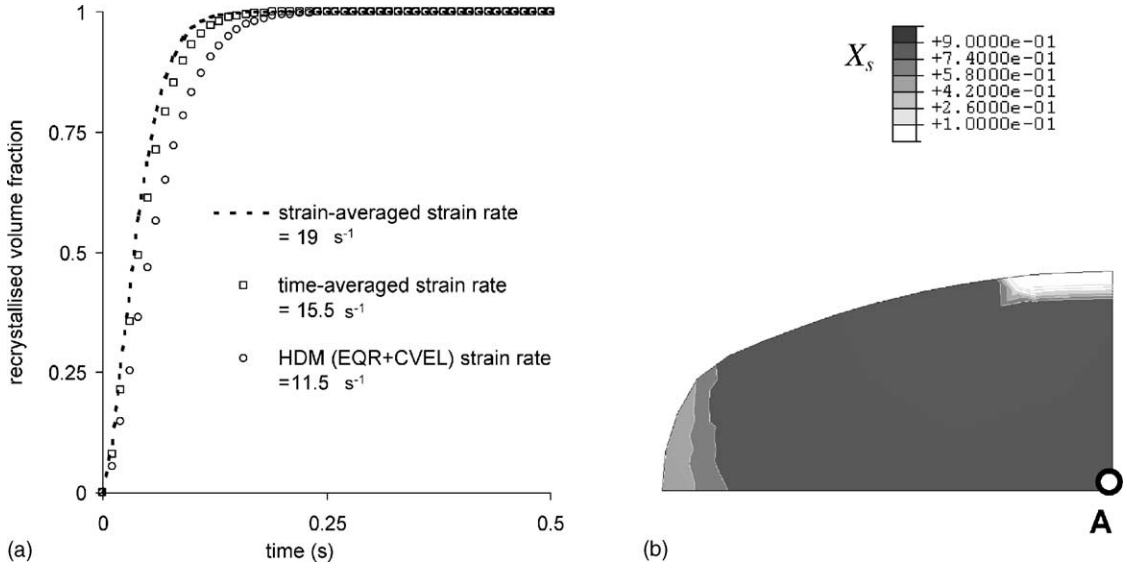

Fig. 6. Evolution of the recrystallised volume fraction X_s in the R8–R9 interstand; $\phi = 24$ mm bar rolling schedule, with R8 stand parameters: $T = 1040\,^{\circ}C$, $V = 1.7\,m\,s^{-1}$; (a) comparison of the X_s predictions resulting from different prior strain rate definitions at location A; (b) cross-sectional distribution at the end of the interstand R8–R9.

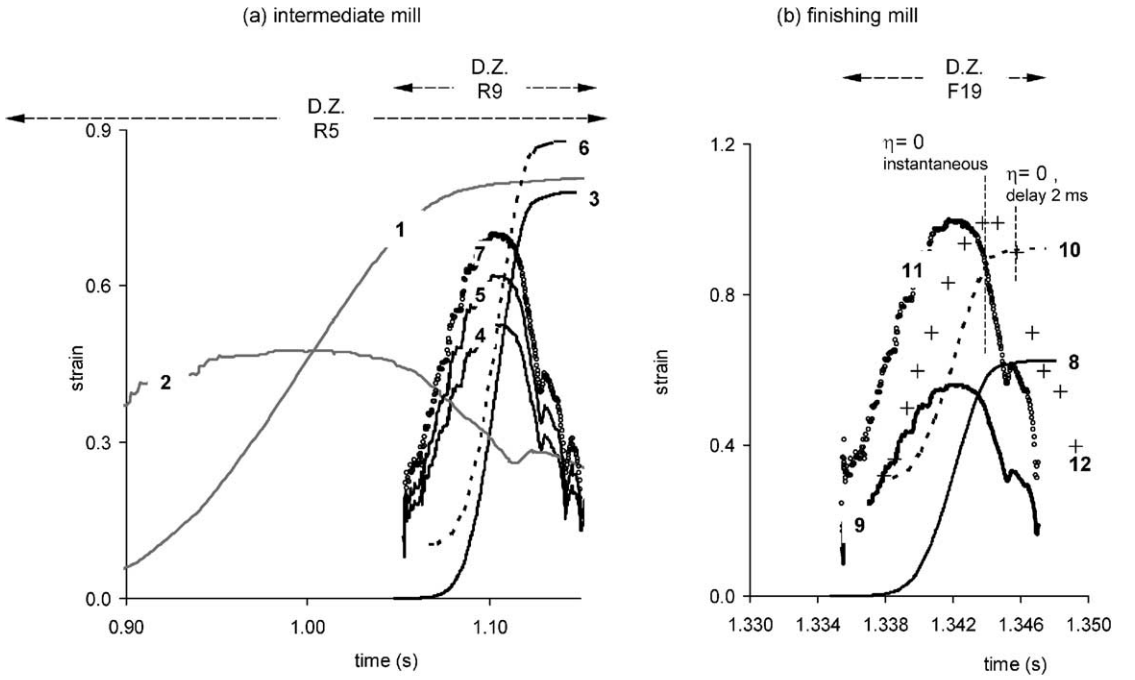

R5 1055 °C, 0.50 m/s		R9 1010 °C, 1.77 m/s		F19 1050 °C, 13 m/s	
1	$\bar{\varepsilon}$ for AR =0.27	3	$\bar{\varepsilon}$ for AR =0.25	8	$\bar{\varepsilon}$ for AR =0.20
2	ε_d for DIN55Cr3, D=60 μm	4	ε_d for DIN55Cr3 , D =36 μm	9	ε_d for DIN55Cr3 , D=24 μm
		5	ε_d for DIN55Cr3 , D =50 μm	10	$\bar{\varepsilon}$ for AR =0.20, accumulated st rain=0.3
		6	$\bar{\varepsilon}$ for AR =0.25, accumulated strain=0.1	11	ε_d for 0.47C-0.66Mn-0.98Cr-0.46Ni-0.97Mo-0.12V-0.016 Nb steel, D=10 μm
		7	ε_d for 0.47C-0.66Mn-0.98Cr-0.46Ni-0.97Mo-0.12V-0.016 Nb steel, D=40 μm	12	hypothetical effect on ε_d: response delayed 2 ms due to microestructural inertia

Fig. 7. Evolution of the pass and DRX strains at the bar's central streamline for different stands, during a ϕ = 5.5 mm rod rolling schedule. Two medium-carbon steels with various grain sizes (AR = area reduction).

= 5.5 mm rod rolling schedule. To prevent excessive adiabatic heating at the finishing mill, the rod schedule starting temperature is lower than for the bar case examined above. The losses due to radiation to the environment and conduction to the rolls occurring in the roughing-intermediate stands are not fully compensated by the conversion of mechanical work into heat due to the lower rolling speeds involved [15,16]. Even though, the associated temperature decrease in the monitored intermediate roughing stands R5 and R9 is not enough to raise the instantaneous ε_d above the exit strain (Fig. 7a) within the span of the deformation zone D.Z., and therefore DRX is predicted. The onset of DRX in R5 occurs very early during the pass strain rise (curves 1 and 2, Fig. 7a). At the R9 stand, DRX starts at higher strains (curves 3–5, Fig. 7a) and for a given steel is delayed by a bigger grain size (curves 4 and 5).

The stands of the subsequent finishing mill runs at higher rolling speed, which generates significant temperature raise due to the reduction of radiation intervals and enhanced heat generation. Fig. 7b shows the predictions of the model for the last stand (F19) of the finishing mill before the sizing block. The resulting ε_d for the studied steel (curve 9, Fig. 7b) is still exceeded by the strain (curve 8) but this happens near the exit of the deformation zone, therefore predicting only a small amount of DRX.

For comparison, predictions for a multialloyed steel (wt.%) 0.47 C, 0.66 Mn, 0.98 Cr, 0.46 Ni, 0.97 Mo, 0.12 V, 0.016 Nb steel, based on the results reported by Kirihata et al. [26], with the coefficients for Eq. (6): $B_2 = 1.36 \times 10^{-3}$, $d = 0.5$, $q = 0.17$, $Q = 241$ kJ mol^{-1} are shown for the R9 (curve 7, Fig. 7a) and F19 stands (curve 11, Fig. 7b). In spite of the higher ε_d values than the base DIN55Cr3 steel for the same rolling conditions, they cannot prevent some DRX in the intermediate mill. In the finishing mill configuration studied, however, the resulting ε_d is overcome by the rolling strain

(curves 8 and 10) only at the exit of the deformation zone, virtually preventing DRX.

8. Discussion

The results of the numerical simulation of hot bar rolling described above clearly indicate the presence of DRX in the bar mill within the context of: (a) immediate response of the microstructure to the new $T - \dot{\bar{\varepsilon}}$ conditions and (b) microstructural evolution dependent on effective $\bar{\varepsilon}$ and $\dot{\bar{\varepsilon}}$ values that consider shear strain reversals.

Even though the volume fraction X_d in Eq. (9) incorporates the changes in both the critical strain ε_d and its DRX kinetics by considering the variations in $T - \dot{\bar{\varepsilon}}$ along the strain path, the whole model does not include any microstructural lagging effect. Should this not be the case and certain amount of inertia in the development of the new microstructure exists, the resulting ε_d will decay at a lower pace. The hypothetical implications of this more realistic scenario are immediate: (i) shifting of the DRX start ($\eta = 0$) towards the D.Z. exit and complete DRX elimination for some finishing configurations and processing conditions (i.e. curve 12, Fig. 7), (ii) a slower SRX kinetics in the following interstand. For the intermediate stands examined (Fig. 7a), however, no changes are expected for both steels because the strain substantially exceeds the instantaneous ε_d.

The extremely short times involved in the decay of $\dot{\bar{\varepsilon}}$ from its maximum value (order 50 ms, in the intermediate roughing stands and up to 13 ms in the finishing stand, Figs. 5 and 7, respectively) are almost impossible to achieve experimentally by a controlled mechanical testing. Separation of material response from the $\dot{\bar{\varepsilon}}$ transient, even at the slower rates the testing allows, should help to quantify or at least bound the amount of microstructural inertia breaking down the instantaneous response assumed in the current model for both microstructure and flow stress.

9. Conclusions

An incremental, isotropic hardening viscoplastic model for hot deformation of medium-carbon steel in the austenite regime has been developed and implemented in a coupled temperature–stress FEM analysis. It has been used to separate the effects of DRX and the work hardening-dynamic recovery processes on the flow stress during compression loading. The flow stress softening due to DRX has been written in terms of thermo-deformation variables and incorporated into the general framework of the incremental constitutive law with a hardness as a state variable. This hypothesis has been validated against results from varying strain rate experiments.

Two prior deformation measures have been identified as most important for computing the degree of softening after varying strain rate deformation by using Eqs. (14–16). They are a time-average of the strain rate (Eq. (19)) for X_d and a SRX–MDRX transition strain obtained from the FEM-material path records the first time the DRX onset condition occurs (Eq. (23)). The first measure has been validated by the results for the recrystallised fractions from the stress relaxation experiments after compression deformation at abruptly changed strain rates. The second measure appears as the natural extrapolation of first appearance of DRX nuclei ($\eta = 0$) to varying-rate loading.

For the medium-carbon steel analysed, the numerical simulation of representative bar/rod rolling passes shows the occurrence of both DRX and MDRX, in agreement with predictions from HDM ensuring the volume constancy but contrary to the more simplistic HDM assumption often used in plant models. In a medium-carbon multialloyed steel processed under the same rolling schedule, a fraction of DRX can be present in the intermediate mill, but is prevented in the last rod finishing stands.

Acknowledgments

This work was supported by the ECSC Steel RTD Programme with Grant no. 7210-PR291. Dr. M. Somani at the University of Oulu is thanked for his careful analysis of numerous Gleeble tests performed. Ing. F. Dionisi Vici at CSM assisted in the FEM implementation of the models.

References

[1] T.M. Maccagno, J.J. Jonas, Correcting the effects of static and metadynamic recrystallisation during the laboratory simulation of rod rolling, ISIJ Int. 34 (7) (1994) 607–614.
[2] T.M. Maccagno, J.J. Jonas, P.D. Hodgson, Spreadsheet modelling of grain size evolution during rod rolling, ISIJ Int. 36 (6) (1996) 720–728.
[3] S. Choi, Y. Lee, P. Hodgson, J.S. Woo, Feasibility study of partial recrystallisation in multi-pass hot deformation and application to calculation of mean flow stress, J. Mater. Process. Technol. 125–126 (2002) 63–71.
[4] Y. Lee, S. Choi, P.D. Hodgson, Integrated model for thermo-mechanical controlled process in rod (or bar) rolling, J. Mater. Process. Technol. 125–126 (2002) 678–688.
[5] S. Serajzadeh, H. Mirbagheri, A. Karimi Taheri, Modelling the temperature distribution and microstructural changes during hot rolling of low carbon steel, J. Mater. Process. Technol. 125–126 (2002) 89–96.
[6] E. Anelli, Application of mathematical modelling to hot rolling and controlled cooling of wire rods and bars, ISIJ Int. 32 (3) (1992) 440–449.
[7] A.J. De Ardo, Fundamental aspects of the physical metallurgy of thermomechanical processing of steels, in: I. Tamura (Ed.), Proceedings of the Conference on Physical Metallurgy of Thermomechanical Processing of Steels and Other Metals, THERMEC-88, Tokyo, ISIJ, 1988, pp. 20–29.
[8] A.J. DeArdo, Modelling of deformation processing: wonderful tool or wishful thinking, in: S. Yue (Ed.), Proceedings of the International Symposium of Mathematical Modelling of Hot Rolling of Steel, Metallurgical Society of The Canadian Institute of Mining and Metallurgy, Montreal, 1990, pp. 220–238.
[9] L.P. Karjalainen, J. Perttula, Characteristics of static and metadynamic recrystallization and strain accumulation in hot-deformed

austenite as revealed by the stress relaxation method, ISIJ Int. 36 (6) (1996) 729–736.
[10] P.D. Hodgson, The Metadynamic Recrystallisation of Steels, in: T. Chandra et al. (Eds.), Proceedings of the International Conference on Thermomechanical Processing of Steels and Other Materials, THERMEC-97, The Minerals, Metals and Materials Society, 1997, pp. 121–131.
[11] L. Anand, Constitutive equations for rate dependent deformation of metals, ASME J. Eng. Mater. Technol. 104 (1982) 12–17.
[12] J.H. Bianchi, J.J. Urcola, Development of a model for hot strip rolling of stainless duplex and non oriented magnetic steels, in: Technical Steel Research Final Report EUR 18378, Official Publications of the EU, Luxembourg, 1998.
[13] J.H. Bianchi, Coupling of microstructural rate effects with the Mechanics of rolling deformation, in: D.R.J. Owen, et al. (Ed.), Proceedings of the Fifth International Conference on Computational Plasticity, Cimme Press, Barcelona, 1997, pp. 1276–1283.
[14] M. Zhou, O. Wiklund, L.P. Karjalainen, J.H. Bianchi, I. Gutierrez, P. Peura, The effect of strain reversal and strain-time path on constitutive relationships for metal rolling/forming processes, in: Technical Steel Research Final Report EUR 19891, Official Publications of the EU, Luxembourg, 2001.
[15] J.H. Thorp, J.H. Bianchi, B. Dahm, D. Mehren, C.P. Johnson, F. Dionisi Vici, Development of systems to aid flexible rolling of long products to closer tolerances by on-line calculation of loaded roll gap, control of stand speed and reheat, in: Technical Steel Research Final Report EUR 20473, Official Publications of the EU, Luxembourg, 2002.
[16] J.H. Bianchi, F. Dionisi, Effects of temperature, rolling speed and preset variations on the loaded roll gap response of a bar mill stand, in: C. Genzano (Ed.), Proceedings of the 14th Rolling Conference, The IAS, Buenos Aires, 2002, pp. 103–112.
[17] S.B. Brown, K. Kim, L. Anand, An internal variable constitutive model for hot working of metals, Int. J. Plast. 5 (2) (1989) 95–130.
[18] HKS, ABAQUS User's Manual, Version 6.2, 2002.
[19] L.P. Karjalainen, Stress relaxation method for investigation of softening kinetics in hot deformed steels, Mater. Sci. Technol. 11 (6) (1995) 557–565.
[20] Y. Estrin, H. Mecking, A unified phenomenological description of work hardening and creep based on one-parameter models, Acta Metall. 32 (1) (1984) 57–70.
[21] J.H. Bianchi, A viscoplastic constitutive law with internal variables for multipass hot rolling, in: Proceedings of the Fourth International Conference on Computational Plasticity, Pineridge Press, Barcelona, 1995, pp. 2283–2292.
[22] Y. Lee, Calculating model of mean strain in rod rolling process, ISIJ Int. 39 (9) (1999) 961–964.
[23] Y. Lee, H.J. Kim, S.M. Hwang, Analytic model for the prediction of mean effective strain in rod rolling process, J. Mater. Process. Technol. 114 (2001) 129–138.
[24] L.P. Karjalainen, D. Porter, P. Peura, Recrystallization of Ti-microalloyed steels under constant and varying deformation conditions, in: Proceedings of the Fourth International Conference on Recrystallization and Related Phenomena, Proceedings of ReX'99, JIMIS-10, 1999, pp. 721–726.
[25] L.P. Karjalainen, M.C. Somani, P. Peura, D. Porter, Effects of strain rate changes and strain path on flow stress and recrystallization kinetics in Nb-bearing microalloyed steels, in: Procedings of the International Conference on Thermomechanical Processing of Steels, London, IOM, 2000, pp. 130–139.
[26] A. Kirihata, F. Siciliano, T.M. Maccagno, J.J. Jonas, Mathematical modelling of mean flow stress during the hot rolling of multialloyed medium-carbon steels, ISIJ Int. 38 (2) (1998) 187–195.